I&EC research
Industrial & Engineering Chemistry Research

Article

Cite This: Ind. Eng. Chem. Res. 2018, 57, 751−767

pubs.acs.org/IECR

Thermodynamic Modeling and Simulation of Biodiesel Systems at Supercritical Conditions

Pedro F. Arce,* Nian F. Vieira, and Edson M. S. Igarashi

Chemical Engineering Department, Engineering School of Lorena, University of São Paulo, Lorena, São Paulo, Brazil

ABSTRACT: Biodiesel is becoming a promising fuel in many markets in the world for being a renewable energy source and for not requiring significant adaptation in existing diesel engines. It is biodegradable and its polluting gas emissions are less harmful to the environment. Transesterification is used for the biodiesel synthesis at supercritical conditions using triacylglycerols and solvents in a heterogeneous reaction. The Peng−Robinson (PR), the volume-translated Peng−Robinson (VT-PR), and the perturbed chain statistical associating fluid theory (PC-SAFT) equations of state were using to predict the fluid phase behavior of systems containing solvents and components present in the synthesis of biodiesel at supercritical conditions. Two pure component parameters for the VT-PR equation, N and k_3, and the five pure component parameters for the PC-SAFT equation, m, σ, and ε as well as the associating parameters $\kappa^{A_iB_j}$ and $\varepsilon^{A_iB_j}$, were predicted based on the vapor pressures and the saturated liquid volumes. Results were compared with experimental data presented in the literature, considered thermodynamically consistent, and it was confirmed that noncubic equations of state are more accurate than cubic equations of state. Thermodynamic modeling was also compared with the thermodynamic simulation using artificial neural networks (ANN) and molecular descriptors at different architectures. Results, in terms of deviations of bubble pressures of and vapor phase composition, predicted by the optimum ANN model are slightly more efficient than the ones obtained by the thermodynamic models, mainly the PC-SAFT equation of state.

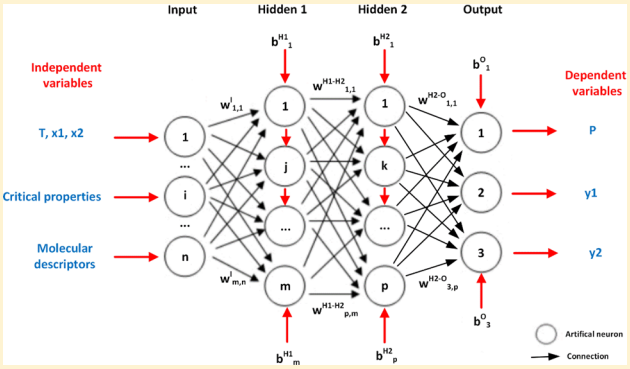

1. INTRODUCTION

1.1. Biodiesel. Many substitutes for diesel fuel have been studied recently, such as the use of vegetable oil or mixtures between oil and diesel, microemulsions of vegetable oil in diesel, and the synthesis of new fuels with pyrolysis and transesterification.[1] Due to its similar properties in comparison with the diesel from petroleum, biodiesel, obtained in transesterification reactions, is considered the most promising substitute.[2] The use of biodiesel is advantageous to the environment in comparison with the use of common diesel, because biodiesel has few sulfur-based and aromatic compounds, it is biodegradable, and because of the fact that carbon emitted in its combustion is balanced with carbon absorbed during the growth of the plants that provide oil.[3]

Biodiesel can be produced with the use of homogeneous catalysts and without them. The method without catalysts is based on the properties of the solvent in supercritical conditions so that, at appropriate temperature and pressure, the solubility of the solvent is reduced to near the value of the solubility of the triacylglycerol, permitting the formation of a homogeneous phase which will increase the reaction efficiency.[3] When the reagents are in a single phase in the reactor, there is no mass transference between interfaces to limit the reaction conversion.[4]

For the synthesis of the biodiesel process, in which many compounds are in equilibrium in the system, the prediction of the behavior of multicomponent systems tends to be useful for a better efficiency of the process or for a better selection of raw material that will be used. However, first it is necessary that the mathematical model fits into simple systems, such as binary systems.[5]

In this work, the term "biodiesel component" is used to refer to fatty acid, fatty acid ester, triacylglycerol, or glycerol and "biodiesel system" is a binary system involving a biodiesel component and supercritical solvent.

1.2. Artificial Neural Networks (ANN). Based on behavior of natural neural networks, artificial neural networks are constituted by layers that consist of a certain number of units, similar to neurons, called nodes. The information introduced in the first layer (stimulus) is transmitted ahead through connections (links) between nodes[6] (Figure 1). Different architectures are obtained according to the topology and search algorithms used. There are four elements present in a typical ANN: (1) a node as a unit that activates when a input signal is received, (2) nodes interconnected between them, (3) a activation function inside a node to transform input into output, and (4) a learning function to manage weights of input−output pairs.[7] The last element is important to minimize certain criterion using a set of allowed

Received: October 9, 2017
Revised: December 10, 2017
Accepted: December 18, 2017
Published: December 18, 2017

DOI: 10.1021/acs.iecr.7b04195
Ind. Eng. Chem. Res. 2018, 57, 751−767

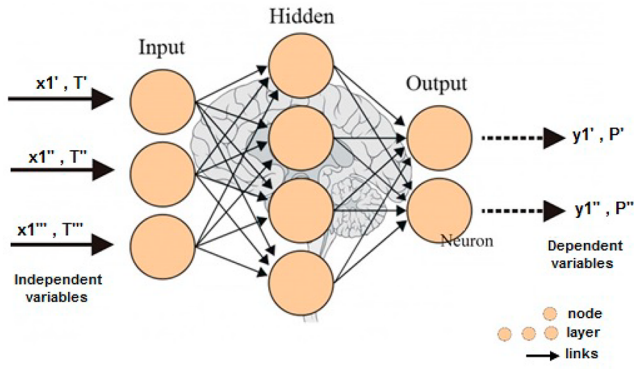

Figure 1. Scheme of artificial neural networks.

models. The Levenberg−Marquardt back-propagation training algorithm, available in MatLab, is the most employed search algorithm for the learning process.[8]

1.3. Molecular Descriptors (MD). Molecular descriptors are fundamental tools in several areas such as quality control, pharmaceutical sciences, health research, chemistry, and other more. They translate some properties of a molecule into numbers allowing an easy mathematical treatment of chemical information that is previously encoded into symbolic representation. Through logic and mathematical functions, the codes of the molecules are transformed to numerical values by standardized experiments.[9] Predominantly, MD are classified as topological indexes, and constitutional, geometrical, and thermodynamic descriptors among many existing classifications. All of them consider attributes such as shape, number of atoms, atom type, molecular size, bound count, ring count, molecular weight, and connectivity of atoms in molecules, along with others. Thermodynamic descriptors, commonly, cover chemical properties in terms of chemical behavior based on heat formation, molar refractivity, etc.[10]

One of the most important programs for calculating MD is Dragon 7.0.[11] It contains more than 5000 molecular descriptors divided into 30 logical blocks allowing an easy retrieval of MD. In this study, Dragon 7.0 was used to obtain MD of biodiesel components. The last version of this computer program allows calculating disconnected structures, i.e., salts, mixtures, ionic liquids, metal complexes, and sequences of metabolites that can be generated by substances. To generate MD, Dragon 7.0 requires determined files to describe the molecular structure and are obtained by specific chemical drawing programs. The most used format for these files is called SMILES (.smi).

1.4. SMILES Codes. SMILES (Simplified Molecular Input Line Entry System) is a line notation that contains the same information on an extended connection table, in a compact way, to represent a chemical structure. SMILES codes translate three-dimensional chemical structure (atoms, bonds, etc.) in a sequence of symbols that is recognized by computer software. SMILES notation is used to enter a chemical structure into EPI Suite estimation programs and ECOSAR. Several software programs are available to translate a chemical structure into SMILES.[12,13]

In this work, first, the pure component parameters of the VT-PR and PC-SAFT models were predicted using the vapor pressures and the saturated liquid volumes. Second, the thermodynamic consistency was applied to the experimental data. Data, considered thermodynamically consistent, were used in the thermodynamic modeling. Third, the fluid phase behaviors, in terms of performance obtained by the thermodynamic modeling and the thermodynamic simulation, were compared. For the thermodynamic modeling, the Peng−Robinson, the volume-translated Peng−Robinson, and the perturbed chain statistical associating fluid theory equations of state were used to describe the vapor−liquid equilibrium in terms of deviations in bubble pressure and the vapor phase composition. The noncubic EoS (PC-SAFT) was more accurate than the cubic equations of state (PR and VT-PR). For the thermodynamic simulation, the proposal of the present research includes using ANN with several architectures with the following independent variables: critical properties of the biodiesel components and supercritical solvents, temperature, and liquid phase composition. Due to the complexity of the fatty acid esters, it was necessary to use molecular descriptors for these solutes, obtained with Dragon 7.0, as independent variables. Dependent variables in the simulation were system pressure and the vapor phase composition. It is necessary to emphasize that, although the simulation using artificial neural networks is a well-known technique, in the case of the fluid behavior of the vapor−liquid equilibrium (VLE), there are no research works using ANN and molecular descriptors for studying the fluid behavior of the VLE of binary systems involving components present in the biodiesel.

2. METHODOLOGY

2.1. Thermodynamic Models. *2.1.1. Peng−Robinson (PR) Equation of State.* The PR EoS[14] can be written with the following form:

$$P = \frac{RT}{\underline{V} - b} - \frac{a}{\underline{V}(\underline{V} + b) + b(\underline{V} - b)} \tag{1}$$

PR EoS constants, a and b, are calculated with the following mixing rules (vdW2) and their combining rules:

$$a = \sum_{i}^{c}\sum_{j}^{c} x_i x_j a_{i,j} \quad \text{and} \quad a_{i,j} = (1 - k_{ij})\sqrt{a_i a_j} \tag{2}$$

$$b = \sum_{i}^{c}\sum_{j}^{c} x_i x_j b_{i,j} \quad \text{and} \quad b_{i,j} = \frac{1}{2}(b_i + b_j)(1 - l_{ij}) \tag{3}$$

where k_{ij} and l_{ij} are adjustable binary parameters. Pure component parameters (a_i and b_i) are calculated from pure component critical properties:

$$a_i = 0.4572 a_{(T_r)i}(RT_{c,i})^2/P_{c,i}; \qquad b_i = 0.0778 RT_{c,i}/P_{c,i} \tag{4}$$

where $a_{(T_r)i} = [1 + m_i(1 - \sqrt{T_{r,i}})]^2$ and parameter m_i is defined in terms of acentric factor (w_i) of component i, as

$$m_i = 0.3746 + 1.5423 w_i - 0.2699 w_i^2 \tag{5}$$

2.1.2. Volume-Translated Peng−Robinson Equation of State. The accuracy of Peng−Robinson equation of state can be improved using a term t_i to correct the calculated value of volume, as is shown in eq 6.

$$V = V_{calc} + t_i \tag{6}$$

With this new parameter, the equation of Peng−Robinson with the volume-translated term (PR-VT)[15] becomes

$$P = \frac{RT}{v + t - b} - \frac{a(T)}{(v + t)(v + b) + b(v + t - b)} \tag{7}$$

DOI: 10.1021/acs.iecr.7b04195
Ind. Eng. Chem. Res. 2018, 57, 751−767

VT-PR EoS constants, a and b, are calculated with the same mixing rules (vdW2) and their combining rules in the same way as in the Peng−Robinson EoS. Constant t is calculated as

$$t = \sum_{i}^{c} x_i t_i \tag{8}$$

Pure component parameters a_i and b_i are calculated by eq 4. Parameters $\alpha_{(T_r)i}$, m_i, and t_i are defined as

$$\alpha_{(T_r)i} = [1 + m_i(1 - T_{r,i}) + N(1 - T_{r,i})(0.7 - T_{r,i})]^2 \tag{9}$$

$$m_i = 0.20473 + 0.83548\omega_i - 0.18470{\omega_i}^2 + 0.16675{\omega_i}^3 - 0.09881{\omega_i}^4 \tag{10}$$

$$t_i = \frac{RT_c}{P_c}[k_1 + k_2(1 - {T_{r,i}}^{2/3}) + k_3(1 - {T_{r,i}}^{2/3})^2] \tag{11}$$

where $T_{r,i}$ is the reduced temperature of component i; N and k_3 are the pure component parameters obtained with vapor pressure and specific volume of saturated liquid data. Parameters k_1 and k_2 are calculated as

$$k_1 = 0.00185 + 0.00438\omega_i + 0.36322{\omega_i}^2 - 0.90831{\omega_i}^3 + 0.55885{\omega_i}^4 \tag{12}$$

$$k_2 = -0.00542 - 0.51112k_3 + 0.04533{k_3}^2 + 0.07447{k_3}^3 - 0.03811{k_3}^4 \tag{13}$$

2.1.3. Perturbed Chain Statistical Associating Fluid Theory (PC-SAFT). PC-SAFT EoS[16,17] calculates the residual Helmholtz energy, $\tilde{a}^{res}$, from the summation of three terms: a reference hard-sphere chain contribution ($\tilde{a}^{hc}$), a perturbation contribution, $\tilde{a}^{pert}$, and an associating contribution, $\tilde{a}^{assoc}$, where $\tilde{a} = A/NkT$. The hard-sphere chain contribution was provided by Chapman and co-workers.[18,19] It was based on the first-order thermodynamic perturbation theory and depends on the radial pair distribution function for segments in the hard-sphere system (g^{hs}) and on the mean segment number ($\bar{m}$), and it is a function of m, the number of segments per chain. The hard-sphere contribution ($\tilde{a}^{hs}$) and the radial distribution function (g_{ij}^{hs}) depend also on the temperature-dependent segment diameter (d_i), which depends directly on the segment diameter (σ) and the depth pair potential (ε), according to

$$d_i = \sigma_{ii}\left[1 - 0.12\exp\left(-3\frac{\varepsilon_{ii}}{kT}\right)\right] \tag{14}$$

The perturbation contribution[20] is calculated from the first ($\tilde{a}_1$) and second-order ($\tilde{a}_2$) perturbation terms, which contain mixing rules in the form of

$$\overline{m_{i,j}\varepsilon_{i,j}^{l}\sigma_{i,j}^{k}} = \sum_{i}^{n_c}\sum_{j}^{n_c} x_i x_j m_i m_j \left(\frac{\varepsilon_{ij}}{kT}\right)^l \sigma_{ij}^k \tag{15}$$

Conventional combining rules are used to determine the cross parameters:

$$\sigma_{ij} = \frac{1}{2}(\sigma_{ii} + \sigma_{jj}) \tag{16}$$

$$\varepsilon_{ij} = \sqrt{\varepsilon_{ii}\varepsilon_{jj}}(1 - k_{ij}) \tag{17}$$

where k_{ij} is an adjustable binary parameter. Here, m_i, σ_{ii}, and ε_{ii} are the pure component parameters of the component i for the PC-SAFT model. When associating compounds are used, it is necessary to add a term to take in account the contribution due to association ($\tilde{a}^{assoc}$),[21] which contain two other pure component parameters: the associating volume parameter, $\kappa^{A_iB_i}$, and the associating energy parameter, $\varepsilon^{A_iB_i}$. Specific details of the PC-SAFT EoS can be found in the scientific literature.[21,22]

2.1.4. Fluid Phase Behavior of the Vapor−Liquid Equilibrium. For obtaining an appropriate thermodynamic model for binary systems, it is fundamental to evaluate the fluid phase behavior of mixtures in the reactive environment, besides permitting the calculations of their properties with their composition in a certain moment of the process. Considering, in the reactor to biodiesel production, in which will exist phase equilibrium between the components, the thermodynamic model proposed will be based on the fugacity equality between the liquid and vapor phases to a certain component i, according to eq 18.

$$\hat{f}_i^{L} = \hat{f}_i^{V} \tag{18}$$

The fugacity of each phase is calculated from the $\phi-\phi$ approach:[23]

$$\hat{f}_i^{L} = x_i\hat{\phi}_i^{L}P \tag{19}$$

$$\hat{f}_i^{V} = y_i\hat{\phi}_i^{V}P \tag{20}$$

where x_i and y_i are the fluid compositions in liquid and vapor phases, respectively. $\hat{\phi}_i$ is the fugacity coefficient of the component i in liquid or vapor phase and can be obtained from the fundamental relationship:[24]

$$RT\ln\hat{\phi}_i = \int_V^\infty \left[\left(\frac{\partial P}{\partial n_i}\right)_{T,\underline{V},n_j} - \frac{RT}{V}\right]dV - RT\ln(Z) \tag{21}$$

The term $\left(\frac{\partial P}{\partial n_i}\right)_{T,\underline{V},n_j}$ depends on the EoS. In eq 21, n is the mole number, P is the pressure, T is the temperature, V is the molar volume, and Z is the compressibility factor. In this work, the fugacity coefficient was calculated numerically by using finite difference and numerical integration methods.[21,25]

2.1.5. Thermodynamic Consistency. Testing the thermodynamic consistency of experimental data is necessary before any thermodynamic modeling process, due to some differences found between data of a given system studied under the same conditions by different researchers.[26,27] Based on the Gibbs−Duhem equation in the most cases, different forms of manipulating this equation create different tests.[28−30]

In this work, an integral or area test[26] from the integral form of the Gibbs−Duhem equation, eq 22, is used because it is a suitable test for isothermal systems with solute present in very small fractions in the vapor phase and under higher pressures.

$$\int\frac{1}{Py_2}\,dP = \int\frac{1 - y_2}{y_2(Z - 1)}\frac{d\hat{\phi}_1}{\hat{\phi}_1} + \int\frac{1}{Z - 1}\frac{d\hat{\phi}_2}{\hat{\phi}_2} \tag{22}$$

where y_2 is the vapor molar fraction of the solute. The compressibility factor, Z, of the vapor phase is used and, with the fugacity coefficients, $\hat{\phi}_i$, is calculated by using the PR EoS[14] combined with the van der Waals mixing rule with one binary interaction parameter, k_{ij}. For the calculations, k_{ij} was adopted

DOI: 10.1021/acs.iecr.7b04195
Ind. Eng. Chem. Res. 2018, 57, 751−767

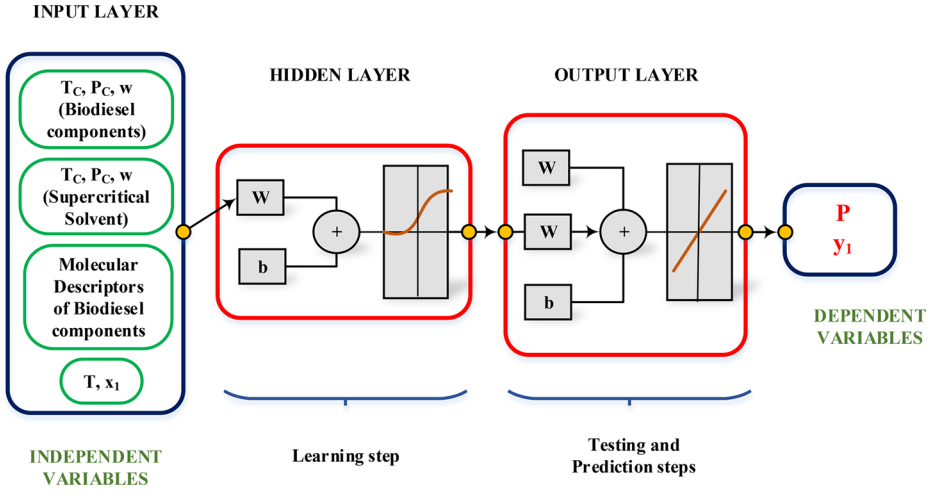

Figure 2. Architecture for artificial neural networks.

equal to zero, so that the mixing rule did not influence in the treatment of the thermodynamic data. Each side of eq 22 will generate an area term called A_P, the term generated by the left side, and A_ϕ, the term generated by the right side, as shown in eq 23.

$$A_P = \int \frac{1}{Py_2}\,dP,$$

$$A_\phi = \int \frac{1-y_2}{y_2(Z-1)}\frac{d\hat{\phi}_1}{\hat{\phi}_1} + \int \frac{1}{Z-1}\frac{d\hat{\phi}_2}{\hat{\phi}_2} \quad (23)$$

From these relationships, the individual percentage, $\%\Delta A_i$, shown in eq 24, correlates the calculated areas for each experimental data set.

$$\%\Delta A = 100\left(\frac{A_\phi - A_P}{A_P}\right) \quad (24)$$

In this case, to determine the thermodynamic consistency of the data, the adopted criterion was that a set of experimental data will be considered consistent if $\%\Delta A_i$ is within the range of values −20 to 20%, while it will be considered inconsistent for values out of the same interval. Numerical method techniques were used to solve eq 23; that is, one point depended on the previous one so that the given segment generated the area corresponding to the integral. Therefore, the test was performed on the experimental data arranged in ascending order considering that the first data was consistent. Only the data considered thermodynamically consistent will proceed for thermodynamic modeling.

2.1.6. Thermodynamic Simulation with Artificial Neural Networks. The fluid phase behavior of binary systems containing compounds present in the production of biodiesel was analyzed by means of the bubble point method at high pressures to study the capability of ANN in learning, testing, and predicting steps, with the dependent variables of system pressure and vapor phase composition. Independent variables were the critical properties of compounds involved in biodiesel systems, system temperature, and liquid phase composition (Figure 2). Due to the uncertainties of some critical properties of some fatty acid esters found in the literature, molecular descriptors were used to improve the accuracy of the independent variables. First, the SMILES code for each molecule of the biodiesel component was found. Second, using Dragon 7.0,[11] numeric values for the 20 molecular descriptors (Table 1) were obtained.

For the learning, testing, and predicting of the fluid phase behavior of biodiesel systems, a spreadsheet file (MS Excel) with six worksheets, each one with a special function, was created. The first, third, and fifth worksheets for the learning, testing, and prediction steps, respectively, contain the independent variables. The second, fourth, and sixth worksheets for the learning, testing, and prediction steps, respectively, contain the dependent variables. Data and the number of data are different for all the worksheets. A computer program for two dependent variables, in MatLab, was developed by our research group[31] that interacts with each worksheet of the spreadsheet file. A friendly version of this software can be downloaded from the following link: http://easyann.gvilella.me/.

In the learning step, the computer program reads the input data, sets the architecture that normally involves a back-propagation feed-forward neural network containing a determined number of layers and generates the weight and bias matrices, and stores such data for the testing step. In the testing step, the computer program reads the weight and bias matrices and the data of the third worksheet which contains the independent variables of biodiesel systems to be learned, and run a number of times, defined by the user, storing all the results in the fourth worksheet. From these results, the average absolute deviation and the maximum absolute deviation are evaluated and the user chooses the best run in terms of the lowest maximum absolute deviations for the two dependent variables (system pressure and vapor phase composition). In the prediction step, with the best run chosen, the computer program predicts the values of the dependent variables for the data of the fifth worksheet. Results of the prediction step are stored in the sixth worksheet. In this worksheet, it is possible to compare with the experimental data if the prediction process was successful for the selected architecture. From here, it is possible to predict the fluid phase behavior of biodiesel systems from unknown values of independent variables, without the need to do more experimental trials.

In this form, for obtaining the best architecture, several network architectures were studied following the procedure described above.

3. RESULTS AND DISCUSSION

In this work, the modeling of the thermodynamic behavior of the vapor−liquid equilibrium of several binary systems including

DOI: 10.1021/acs.iecr.7b04195
Ind. Eng. Chem. Res. 2018, 57, 751−767

Table 1. Molecular Descriptors from Dragon 7.0 used in this work

molecular descriptor	name	subblock	block
MW	molecular weight	basic descriptors	constitutional indexes
AMW	average molecular weight		
nH	number of hydrogen atoms		
nC	number of carbon atoms		
nStructures	number of disconnected structures		
Pol	polarity number	distance-based indexes	topological indexes
X1Av	average valence connectivity index of order 1	Kier−Hall molecular connectivity indexes	connectivity indexes
X1SOL	solvation connectivity index	solvation connectivity indexes	
XMOD	modified Randic index	Randic-like connectivity indexes	
RDCHI	reciprocal distance sum Randic-like index		
P_VSA_p_1	P_VSA-like polarizability, bin 1	polarizability	P_VSA-like descriptors
nHDon	number of donor atoms for H-bonds	basic descriptors	functional group counts
nHAcc	number of acceptor atoms for H-bonds (N, O, F)		
nRCOOH	number of carboxylic acids (aliphatics)		
nRCOOR	number of esters (aliphatics)		
SAacc	surface area of acceptor atoms from P_VSA-like descriptors		
SAtot	surface area (total)		
VvdwMG	van der Waals volume for McGowan volume	basic descriptors	molecular properties
PDI	packing density index		
TPSA(ToT)	topological polar surface area using N, O, S, P polar contributions		

Table 2. Physical Characteristics of Binary Systems Involving Biodiesel Components

system	NP	ΔT [K]	ΔP [MPa]	Δx_1	Δy_1
Solvent + Triacylglycerol					
CO_2 + tricaprilin[32]	10	333.2−353.2	5.33−25.00	0.6915−0.9492	0.9887−0.9999
CO_2 + tripalmitin[33]	9	333.0−353.0	10.00−50.00	0.6200−0.9280	0.9981−1.0000
CO_2 + tristearin[33]	9	333.0−353.0	20.00−50.00	0.5870−0.9140	0.9987−1.0000
CO_2 + triolein[33]	8	333.0−353.0	20.00−50.00	0.8360−0.9240	0.9988−1.0000
CO_2 + trilaurin[32]	6	353.2	10.28−31.80	0.8189−0.9999	0.9978−1.0000
methanol + triolein[34]	16	473.0−503.0	2.86−5.49	0.8207−0.9849	0.9995−1.0000
Solvent + Fatty Acid					
CO_2 + caproic acid[32]	10	313.2−353.2	2.72−15.88	0.1709−0.9110	0.9644−0.9999
CO_2 + lauric acid[32]	16	333.2−353.2	2.57−27.65	0.2471−0.8929	0.9593−0.9999
CO_2 + palmitic acid[32]	7	353.2−373.2	13.60−30.52	0.5771−0.8082	0.9973−0.9999
Solvent + Fatty Acid Ester					
CO_2 + ethyl stearate[35]	29	313.2−333.2	1.47−18.26	0.3270−0.9120	0.9850−1.0000
CO_2 + ethyl oleate[35]	37	313.2−333.2	1.14−18.62	0.1950−0.9610	0.9770−1.0000
CO_2 + ethyl linoleate[35]	32	313.2−333.2	1.97−16.97	0.2990−0.9470	0.9810−1.0000
CO_2 + DHA ethyl ester[35]	26	313.2−333.2	1.87−19.22	0.4826−0.9040	0.9878−0.9999
CO_2+ EPA ethyl ester[35]	33	313.2−333.2	2.01−19.04	0.5081−0.9232	0.9806−0.9999
ethanol + ethyl myristate[36]	19	493.0−543.0	2.11−6.93	0.4520−0.9280	0.9858−0.9998
ethanol + ethyl laurate[36]	22	493.0−543.0	2.23−7.09	0.4390−0.9410	0.9657−0.9996
methanol + methyl laurate[37]	20	493.0−543.0	2.16−8.49	0.4330−0.8950	0.9800−0.9999
methanol + methyl myristate[37]	19	493.0−543.0	2.41−8.42	0.3900−0.8980	0.9910−0.9999
methanol + C18 methyl esters[38]	15	523.0−573.0	2.45−11.45	0.4650−0.9160	0.9860−1.0000
Solvent + Glycerol					
ethanol + glycerol[39]	22	493.0−573.0	2.27−8.78	0.3160−0.8890	0.9310−0.9999
methanol + glycerol[39]	22	493.0−573.0	3.03−11.01	0.4310−0.9650	0.9630−0.9999

fatty acid esters and supercritical solvents using the PR, VT-PR, and PC-SAFT equations of state, and the thermodynamic simulation by using artificial neural networks with molecular descriptors, were the main goals.

3.1. Physical Characteristics of Biodiesel Systems Studied. Biodiesel systems studied for modeling the fluid phase behavior are shown in Table 2, where NP, ΔT, ΔP, Δx_1, and Δy_1 represent the number of experimental points, temperature, pressure, and liquid and vapor phase compositions (molar fractions), respectively.

3.2. Pure Component Parameters. In Table 3, the critical properties and the acentric factor that are used in the Peng−Robinson and the VT-PR equations of state are presented, while the parameters N and k_3 for the VT-PR EoS are shown in Table 4, which also shows the references of the vapor pressure and density data used to calculate them. Pure component parameters of the PC-SAFT equation of state are also shown in Table 4.

VT-PR and PC-SAFT pure component parameters were obtained by fitting pure component data. Data for vapor pressure

DOI: 10.1021/acs.iecr.7b04195
Ind. Eng. Chem. Res. 2018, 57, 751−767

and liquid molar volumes were considered. The minimization function used in the modified likelihood maximum[52] is

$$\mathrm{OF} = \sum_{i=1}^{\mathrm{NP}} \left[\frac{|P_{\mathrm{exp}}^{\mathrm{sat}} - P_{\mathrm{calc}}^{\mathrm{sat}}|}{P_{\mathrm{exp}}^{\mathrm{sat}}} + \frac{|\rho_{\mathrm{exp}}^{\mathrm{sat}} - \rho_{\mathrm{calc}}^{\mathrm{sat}}|}{\rho_{\mathrm{exp}}^{\mathrm{sat}}} \right] \tag{25}$$

where NP is the number of experimental point data for a given system. The fitted characteristic parameters are then used to calculate the average deviation from the experimental saturated liquid molar volume and saturated vapor pressure:

$$\Delta P = \frac{1}{\mathrm{NP}} \sum_{i=1}^{\mathrm{NP}} \frac{|P_{\mathrm{exp}}^{\mathrm{sat}} - P_{\mathrm{calc}}^{\mathrm{sat}}|}{P_{\mathrm{exp}}^{\mathrm{sat}}} \times 100 \tag{26}$$

$$\Delta v = \frac{1}{\mathrm{NP}} \sum_{i=1}^{\mathrm{NP}} \frac{|v_{\mathrm{exp}}^{\mathrm{L}} - v_{\mathrm{calc}}^{\mathrm{L}}|}{v_{\mathrm{exp}}^{\mathrm{L}}} \times 100 \tag{27}$$

In these equations, "exp" refers to vapor pressure and liquid molar volume data (Table 4). Since the accuracy of the fitting is better over a restricted data range, and since often data and thermodynamic functions at only low and moderate pressures are needed for engineering work, the characteristic parameters are adjusted over an adequate pressure and temperature range. The computational subroutines which calculate EoS pure component parameters have been written considering the possibility of multiple solutions by searching for the optimum parameters over a wide interval of feasible solutions. This method was applied in previous works and the results were very satisfactory.[50−52]

3.3. Thermodynamic Consistency. The results of the thermodynamic consistency test of experimental data studied attended the criteria adopted in the most cases as shown in Table 5,[53] where NPTC is the number of points thermodynamically consistent. The whole data from binary systems containing methanol and ethanol were considered thermodynamically consistent, while some experimental data from systems containing carbon dioxide did not attend the interval adopted as criterion.

3.4. Thermodynamic Modeling. For the thermodynamic modeling of the fluid phase behavior by using the PR and VT-PR equations of state, the two binary interaction parameters, k_{ij} and l_{ij}, are used to adjust the experimental data points with the calculated points. For the PC-SAFT EoS, only one binary interaction parameter, k_{ij}, is used. These parameters are dependent on the temperature and may be expressed by functions with two

Table 3. Critical Properties of the Components Studied in This Work

component	T_c [K]	P_c [MPa]	w
tricaprilin[40]	793.4	0.74	1.050
tripalmitin[40]	923.4	0.37	1.630
tristearin[40]	945.2	0.33	1.730
triolein[40]	954.1	0.36	1.686
trilaurin[40]	869.8	0.49	1.370
caproic acid[41]	660.2	3.31	0.730
lauric acid[41]	743.0	1.94	0.880
palmitic acid[41]	785.0	1.51	0.983
ethyl stearate[42]	775.8	1.12	0.961
ethyl oleate[42]	771.0	1.19	0.992
ethyl linoleate[42]	785.9	1.12	1.008
DHA ethyl ester[43]	867.1	1.01	0.990
EPA ethyl ester[43]	833.8	1.18	1.013
ethyl myristate[42]	744.3	1.40	0.862
ethyl laurate[42]	719.1	1.60	0.787
methyl laurate[44]	712.0	1.74	0.692
methyl myristate[44]	740.0	1.43	0.736
methyl stearate[44]	788.0	1.12	0.864
glycerol[41]	850.0	7.50	0.513
methanol[41]	512.6	8.01	0.566
ethanol[41]	513.9	6.30	0.649
carbon dioxide[41]	304.1	7.38	0.228

Table 4. Pure Component Parameters for the VT-PR and PC-SAFT Models

	VT-PR				PC-SAFT						
component	N	k_3	ΔP	Δv	m/MW (mol^{-1})	σ (10^{10} m)	ε/k (K)	k^{A,B_i}	$\varepsilon^{A,B_i}/k$ (K)	ΔP	Δv
tricaprylin[45]	3.1500	−0.2062	6.61	2.73	11.2365	3.7812	261.25	–	–	1.45	0.12
tripalmitin[45,46]	5.8451	−2.8826	1.84	6.42	14.8521	3.8841	264.87	–	–	1.08	0.09
tristearin[45,46]	6.3987	−3.0225	2.91	9.58	20.5218	3.6548	258.45	–	–	1.34	0.08
triolein[41,45]	6.6467	−3.2452	1.36	9.73	22.4522	3.5478	259.74	–	–	0.89	0.09
trilaurin[45,46]	3.6511	−2.4155	5.59	5.14	12.3654	3.5871	263.85	–	–	1.65	0.13
caproic acid[41]	0.4187	−0.0802	0.55	2.05	3.9314	3.5542	278.84	0.0008	4192.74	1.13	0.08
lauric acid[41]	0.6282	−0.1275	0.19	1.50	5.2214	3.6452	273.65	0.0012	4215.25	1.54	0.07
palmitic acid[41]	0.6024	0.0252	0.28	0.51	6.8742	3.6145	270.25	0.0010	4082.23	2.01	0.09
ethyl stearate[47,48]	1.9262	0.0030	0.00	0.20	10.4875	3.6012	233.74	–	–	1.54	0.06
ethyl oleate[47,48]	1.1753	0.0565	0.00	0.25	8.1748	3.8245	259.25	–	–	0.87	0.07
ethyl linoleate[47,49]	−0.2543	−0.0098	0.00	0.44	9.8123	3.6354	242.78	–	–	0.93	0.05
DHA ethyl ester[50]	−0.7070	−0.2306	0.06	0.36	10.2548	3.7525	248.85	–	–	1.13	0.06
EPA ethyl ester[50]	−1.0792	−0.0724	0.01	0.07	9.8952	3.7012	251.23	–	–	1.32	0.08
ethyl myristate[47,48]	0.0431	−0.1892	0.00	0.51	7.4951	3.8123	251.74	–	–	0.87	0.04
ethyl laurate[47,48]	−0.0690	−0.2525	0.00	0.53	6.8021	3.7548	251.40	–	–	0.54	0.07
methyl laurate[48,51]	0.2968	−0.0764	0.64	1.67	6.5048	3.7285	251.85	–	–	1.14	0.09
methyl myristate[48,51]	0.2847	−0.2608	0.00	0.23	7.0942	3.7815	252.48	–	–	1.23	0.13
methyl stearate[48,51]	0.3779	−0.3799	0.12	0.67	8.8541	3.7748	251.07	–	–	0.87	0.11
glycerol[41]	0.6069	0.1826	0.13	0.50	1.5815	4.1560	552.74	0.0004	4359.44	0.69	0.04
methanol[15,41]	0.0322	−0.0443	–	–	1.5023	3.2105	189.45	0.0347	2875.52	1.32	0.05
ethanol[15,41]	0.2076	0.0269	–	–	2.3541	3.1865	197.51	0.0329	2664.03	0.89	0.02
carbon dioxide[15,41]	0.1133	0.2900	–	–	2.0514	2.8145	168.74	–	–	0.54	0.00

DOI: 10.1021/acs.iecr.7b04195
Ind. Eng. Chem. Res. 2018, 57, 751−767

Table 5. Results for the Thermodynamic Consistency of Biodiesel Systems

system	T [K]	NP	NPTC	system	T [K]	NP	NPTC
CO_2 + tricaprilin	333.2	4	4	methanol + triolein	473.0	4	4
	353.2	6	6		483.0	4	4
CO_2 + tripalmitin	333.0	4	1		493.0	4	4
	353.0	5	3		503.0	4	4
CO_2 + tristearin	333.0	5	4	methanol + methyl laurate	493.0	7	7
	353.0	4	2		523.0	6	6
CO_2 + triolein	333.0	4	1		543.0	7	7
	353.0	4	3	methanol + methyl myristate	493.0	6	6
CO_2 + trilaurin	353.2	6	6		523.0	6	6
CO_2 + caproic acid	313.2	4	4		543.0	7	7
	353.2	6	6	methanol + methyl stearate	523.0	5	5
CO_2 + lauric acid	333.2	10	10		548.0	5	5
	353.2	6	6		573.0	5	5
CO_2 + palmitic acid	353.2	3	3	methanol + glycerol	493.0	6	6
	373.2	4	4		523.0	5	5
CO_2 + ethyl stearate	313.2	9	9		543.0	6	6
	323.2	9	9		573.0	5	5
	333.2	11	11				
CO_2 + ethyl oleate	313.2	8	8				
	323.2	13	13	ethanol + glycerol	493.0	6	6
	333.2	16	16		523.0	5	5
CO_2 + ethyl linoleate	313.2	8	7		543.0	6	6
	323.2	11	11		573.0	5	5
	333.2	13	13	ethanol + ethyl laurate	493.0	6	6
CO_2 + DHA ethyl ester	313.2	11	10		523.0	8	8
	323.2	9	9		543.0	8	8
	333.2	7	7	ethanol + ethyl myristate	493.0	6	6
CO_2 + EPA ethyl ester	313.2	10	9		523.0	6	6
	323.2	10	10		543.0	7	7
	333.2	13	13				

Table 6. Results of Binary Systems: Supercritical Solvent + Triacylglycerol

		k_{ij}		l_{ij}			
system	EoS	A	B	A'	B'	Δy_1	ΔP
CO_2 + tricaprilin	PR	0.0599	−0.0210	0.1677	−0.0071	0.44	2.84
	PR-VT	0.0171	0.0113	0.0996	−0.0028	0.44	2.52
	PC-SAFT	0.2577	−61.1251	–	–	0.08	0.98
CO_2 + tripalmitin	PR[a]						
	PR-VT	0.2772	−86.5622	−0.0957	28.1683	0.08	1.63
	PC-SAFT	0.2227	−53.4852	–	–	0.04	0.35
CO_2 + tristearin	PR[a]						
	PR-VT	0.0180	−0.0012	−0.0174	0.0004	0.05	0.29
	PC-SAFT	0.2799	−75.8192	–	–	0.03	0.12
CO_2 + triolein	PR	0.0475	−0.2357	0.0805	0.1515	0.03	4.61
	PR-VT	0.0212	0.0848	0.0183	−0.0167	0.03	0.17
	PC-SAFT	0.3245	−94.0391	–	–	0.02	0.08
CO_2 + trilaurin	PR	0.0727	–	0.0823	–	0.08	1.78
	PR-VT	0.0432	–	0.0807	–	0.08	1.69
	PC-SAFT	0.0412	–	–	–	0.02	1.85
methanol + triolein	PR	−0.2813	0.0003	−0.4837	−0.0011	0.02	2.08
	PR-VT	−0.3170	0.0010	−0.7139	−0.0018	0.02	3.19
	PC-SAFT	0.2018	−75.6285	–	–	0.01	0.81

[a]It is not possible to reach convergence.

constants, A and B. In this work, for the thermodynamic modeling, eqs 28 and 29 presented the best adjustment, for all binary systems, the dependence of the binary interaction parameter with temperature.

$$k_{ij} = A + \frac{B}{T} \tag{28}$$

$$l_{ij} = A' + \frac{B'}{T} \tag{29}$$

The values of A and B found for the parameters k_{ij} and l_{ij} for each system and the vapor phase composition error (Δy_1) and the system pressure error (ΔP) using the PR, VT-PR, and PC-SAFT equations of state are shown in

DOI: 10.1021/acs.iecr.7b04195
Ind. Eng. Chem. Res. 2018, 57, 751−767

Table 7. Results of Binary Systems: Supercritical Solvent + Fatty Acid

system	EoS	k_{ij}		l_{ij}		Δy_1	ΔP
		A	B	A'	B'		
CO_2 + caproic acid	PR	−0.0900	29.5712	0.1340	−10.5286	16.73	56.91
	PR-VT	0.0204	−0.0077	0.1196	0.0009	18.66	63.04
	PC-SAFT	0.0884	−14.6423	–	–	2.46	3.48
CO_2 + lauric acid	PR	0.0564	0.0649	0.03990	−0.0080	1.42	5.27
	PR-VT	0.0632	0.0015	0.0279	−0.0003	1.40	3.24
	PC-SAFT	0.1347	−31.5124	–	–	0.48	0.87
CO_2 + palmitic acid	PR	0.0715	0.0389	0.0061	−0.0242	0.06	0.94
	PR-VT	0.0780	−0.0121	−0.0012	0.0094	0.06	0.81
	PC-SAFT	0.1696	−41.4762	–	–	0.03	0.27

Table 8. Results of Binary Systems: Supercritical Solvent + Ester

system	EoS	k_{ij}		l_{ij}		Δy_1	ΔP
		A	B	A'	B'		
CO_2 + ethyl stearate	PR	0.0550	0.0005	0.0657	0.0001	0.81	3.79
	PR-VT	0.0213	0.0006	0.0333	−0.0041	0.58	2.24
	PC-SAFT	0.1884	−42.4412	–	–	0.13	0.74
CO_2 + ethyl oleate	PR	0.0504	−0.0002	0.0469	0.0003	1.01	1.79
	PR-VT	0.0400	−0.0176	0.0302	0.0017	0.90	1.13
	PC-SAFT	0.1685	−39.8245	–	–	0.32	0.29
CO_2 + ethyl linoleate	PR	0.0451	0.0247	0.0443	−0.0029	1.58	3.78
	PR-VT	0.0835	−0.0168	0.0747	0.0100	2.25	6.50
	PC-SAFT	0.1906	−46.8341	–	–	0.42	0.75
CO_2 + DHA ethyl ester	PR	0.0513	−0.0124	0.0870	0.0045	0.74	2.41
	PR-VT	0.1120	−0.0144	0.1562	0.0044	22.57	79.41
	PC-SAFT	0.1787	−35.1261	–	–	0.09	0.36
CO_2 + EPA ethyl ester	PR	−0.0272	22.2080	0.0781	−1.8923	0.73	2.80
	PR-VT	0.1731	−18.1080	0.1442	3.1771	1.31	3.42
	PC-SAFT	0.3538	−97.4521	–	–	0.12	0.63
ethanol + ethyl myristate	PR	−0.1083	−0.0003	0.2957	0.0007	9.66	66.18
	PR-VT	−0.0878	−0.0004	0.3356	0.0007	10.46	69.98
	PC-SAFT	0.2057	−85.5372	–	–	1.32	1.48
ethanol + ethyl laurate	PR	−0.1968	0.0087	0.2296	0.0029	8.44	51.66
	PR-VT	−0.1779	−0.0016	0.2804	0.0009	9.20	57.11
	PC-SAFT	0.1213	−39.5771	–	–	1.08	2.47
methanol + methyl myristate	PR	0.0959	−0.0024	0.4512	0.0022	16.83	110.57
	PR-VT	0.1040	−0.0098	0.4619	0.0064	16.65	105.47
	PC-SAFT	0.0348	7.5196	–	–	1.25	2.78
methanol + methyl laurate	PR	0.0179	−0.0024	0.4046	0.0023	19.17	101.54
	PR-VT	0.0125	−0.0014	0.3896	0.0016	17.71	89.03
	PC-SAFT	0.1045	−28.5642	–	–	1.87	2.49
methanol + methyl stearate	PR	0.0512	0.0040	0.3317	−0.0003	4.23	25.81
	PR-VT	0.0632	0.0018	0.3587	0.0003	4.49	27.49
	PC-SAFT	0.0061	18.4671	–	–	0.74	1.82

Table 9. Results of Binary Systems: Supercritical Solvent + Glycerol

system	EoS	k_{ij}		l_{ij}		Δy_1	ΔP
		A	B	A'	B'		
ethanol + glycerol	PR	−0.6594	−0.0039	−0.3220	−0.0029	22.37	85.24
	PR-VT	−0.6334	−0.0327	−0.3153	−0.0051	22.57	79.41
	PC-SAFT	−0.0343	38.0623	–	–	1.41	2.73
methanol + glycerol	PR	−0.3916	−0.0071	−0.0745	0.0002	12.57	62.71
	PR-VT	−0.3672	−0.0015	−0.0655	−0.0001	12.76	58.01
	PC-SAFT	0.1479	−56.7821	–	–	1.32	2.53

Tables 6– 9. Deviations were calculated in according with eqs 30 and 31.

$$\Delta y_i = \sum_1^n \frac{|y_{calc} - y_{exp}|}{y_{calc}} \quad (30)$$

$$\Delta P = \sum_1^n \frac{|P_{calc} - P_{exp}|}{P_{calc}} \quad (31)$$

It is possible to see in the tables, for binary systems containing CO_2 and triacylglycerols, that the use of the volume translation in

DOI: 10.1021/acs.iecr.7b04195
Ind. Eng. Chem. Res. 2018, 57, 751−767

Table 10. SMILES Code for the Biodiesel Components

component	SMILES code
tricaprilin	CCCCCCCC(=O)OCC(COC(=O)CCCCCCC)OC(=O)CCCCCCC
tripalmitin	CCCCCCCCCCCCCCCC(=O)OCC(COC(=O)CCCCCCCCCCCCCCC)OC(=O)CCCCCCCCCCCCCCC
tristearin	CCCCCCCCCCCCCCCCCC(=O)OCC(COC(=O)CCCCCCCCCCCCCCCCC)OC(=O)CCCCCCCCCCCCCCCCC
triolein	CCCCCCCC\C=C/CCCCCCCC(=O)OCC(COC(=O)CCCCCCC\C=C/CCCCCCCC)OC(=O)CCCCCCC\C=C/CCCCCCCC
trilaurin	CCCCCCCCCCCC(=O)OCC(COC(=O)CCCCCCCCCCC)OC(=O)CCCCCCCCCCC
caproic acid	CCCCCC(O)=O
lauric acid	CCCCCCCCCCCC(O)=O
palmitic acid	CCCCCCCCCCCCCCCC(O)=O
ethyl stearate	CCCCCCCCCCCCCCCCCC(=O)OCC
ethyl oleate	CCCCCCCC\C=C/CCCCCCCC(=O)OCC
ethyl linoleate	CCCCC/C=C\C\C=C/CCCCCCCC(=O)OCC
DHA ethyl ester	CCCCCCCCCC=CC=CC=CC=CC=CC(=O)OCC
EPA ethyl ester	CC/C=C\C/C=C\C/C=C\C/C=C\C/C=C\CCCC(OCC)=O
ethyl myristate	CCCCCCCCCCCCCC(=O)OCC
ethyl laurate	CCCCCCCCCCCC(=O)OCC
methyl laurate	CCCCCCCCCCCC(=O)OC
methyl myristate	CCCCCCCCCCCCCC(=O)OC
methyl stearate	CCCCCCCCCCCCCCCCCC(=O)OC
glycerol	OCC(O)CO

Table 11. Numeric Values for Molecular Descriptors of the Biodiesel Components

molecular descriptor	MW	AMW	nH	nC	nStructures	Pol	X1Av	X1SOL	XMOD	RDCHI
tricaprilin	470.77	5.672	50	27	1	35	0.423	16.028	100.531	4.588
tripalmitin	807.49	5.210	98	51	1	59	0.456	28.028	172.531	7.037
tristearin	891.67	5.154	110	57	1	65	0.460	31.028	190.531	7.617
triolein	885.61	5.303	104	57	1	65	0.443	31.028	190.531	7.617
trilaurin	639.13	5.371	74	39	1	47	0.444	22.028	136.531	5.842
caproic acid	116.18	5.809	12	6	1	5	0.427	3.770	23.775	1.909
lauric acid	200.36	5.273	24	12	1	11	0.461	6.770	41.775	2.795
palmitic acid	256.48	5.130	32	16	1	15	0.470	8.770	53.775	3.330
ethyl stearate	312.60	5.042	40	20	1	20	0.475	10.808	66.334	3.807
ethyl oleate	310.58	5.176	38	20	1	20	0.458	10.808	66.334	3.807
ethyl linoleate	308.56	5.320	36	20	1	20	0.441	10.808	66.334	3.807
DHA ethyl ester	356.25	5.699	36	24	1	22	0.405	11.808	72.334	4.053
EPA ethyl ester	314.58	5.699	34	22	1	21	0.401	11.808	72.334	4.053
ethyl myristate	256.48	5.130	32	16	1	16	0.469	8.808	54.334	3.298
ethyl laurate	228.42	5.191	28	14	1	14	0.464	7.808	48.334	3.034
methyl laurate	214.39	5.229	26	13	1	13	0.456	7.308	45.541	2.910
methyl myristate	242.45	5.159	30	15	1	15	0.461	8.308	51.541	3.178
methyl stearate	298.57	5.061	38	19	1	19	0.469	10.308	63.541	3.692
glycerol	92.11	6.579	8	3	1	4	0.341	2.808	18.840	1.559

molecular descriptor	P_VSA_p_1	nHDon	nHAcc	nRCOOH	nRCOOR	SAacc	SAtot	VvdwMG	PDI	TPSA(ToT)
tricaprilin	588.555	0	3	0	6	78.900	799.845	108.434	284.959	0.859
tripalmitin	1153.568	0	3	0	6	78.900	1425.687	108.434	515.175	0.876
tristearin	1294.821	0	3	0	6	78.900	1582.148	108.434	572.729	0.878
triolein	1224.195	0	3	0	6	78.900	1553.171	108.434	563.947	0.881
trilaurin	871.062	0	3	0	6	78.900	1112.766	108.434	400.067	0.870
caproic acid	129.482	1	0	1	2	37.300	217.184	67.828	73.390	0.787
lauric acid	270.735	1	0	1	2	37.300	373.644	67.828	130.944	0.833
palmitic acid	364.904	1	0	1	2	37.300	477.951	67.828	169.313	0.847
ethyl stearate	470.844	0	1	0	2	26.300	576.976	36.145	207.682	0.864
ethyl oleate	447.302	0	1	0	2	26.300	567.317	36.145	204.755	0.866
ethyl linoleate	423.760	0	1	0	2	26.300	557.658	36.145	201.828	0.868
DHA ethyl ester	400.217	0	1	0	2	26.300	580.835	36.145	212.230	0.877
EPA ethyl ester	400.217	0	1	0	2	26.300	580.835	36.145	212.230	0.877
ethyl myristate	376.675	0	1	0	2	26.300	472.669	36.145	169.313	0.857
ethyl laurate	329.591	0	1	0	2	26.300	420.515	36.145	150.128	0.852
methyl laurate	306.049	0	1	0	2	26.300	394.438	36.145	140.536	0.848
methyl myristate	353.133	0	1	0	2	26.300	446.592	36.145	159.721	0.854
methyl stearate	447.302	0	1	0	2	26.300	550.899	36.145	198.090	0.862
glycerol	58.856	0	0	3	3	60.690	186.906	128.050	51.536	0.629

DOI: 10.1021/acs.iecr.7b04195
Ind. Eng. Chem. Res. 2018, 57, 751−767

Table 12. Results for *X*−*X*−2 and 3−*X*−*X*−2 Architectures

architecture	iteration	ΔP	Δy_1	architecture	iteration	ΔP	Δy_1
2−3−2	27	5.25	0.89	3−3−5−2	15	5.34	0.35
2−5−2	12	7.43	0.78	3−3−10−2	50	5.04	0.42
2−10−2	7	5.23	1.05	3−3−15−2	6	5.02	0.45
2−15−2	32	6.43	0.85	3−3−20−2	4	5.06	0.44
2−20−2	43	8.67	0.93	3−3−25−2	27	4.87	0.37
2−25−2	2	5.89	0.91	3−3−30−2	30	4.58	0.39
2−30−2	33	6.34	0.97	3−5−5−2	4	4.79	0.31
3−3−2	38	8.78	0.87	3−5−10−2	22	4.87	0.33
3−5−2	48	5.43	0.89	3−5−15−2	15	4.53	0.28
3−10−2	25	6.21	1.05	3−5−20−2	27	4.41	0.27
3−15−2	44	5.87	1.07	3−5−25−2	42	4.67	0.25
3−20−2	13	8.77	1.10	3−5−30−2	49	4.25	0.28
3−25−2	22	5.30	0.89	3−10−5−2	28	4.20	0.29
3−30−2	18	6.34	0.82	3−10−10−2	9	4.38	0.31
5−3−2	20	6.45	0.93	3−10−15−2	8	4.32	0.24
5−5−2	34	5.67	0.98	3−10−20−2	10	4.23	0.29
5−10−2	38	5.89	1.08	3−10−25−2	35	4.12	0.26
5−15−2	8	5.08	0.97	3−10−30−2	44	4.02	0.28
5−20−2	11	5.76	1.09	3−15−5−2	50	4.23	0.32
5−25−2	13	4.53	1.12	3−15−10−2	23	4.26	0.35
5−30−2	44	7.37	0.85	3−15−15−2	29	4.04	0.32
10−3−2	43	4.09	0.88	3−15−20−2	22	4.01	0.33
10−5−2	45	7.68	0.96	3−15−25−2	13	4.08	0.28
10−10−2	26	5.35	0.91	3−15−30−2	24	4.12	0.25
10−15−2	41	6.45	0.90	3−20−5−2	13	4.03	0.24
10−20−2	20	4.34	0.88	3−20−10−2	25	4.06	0.22
10−25−2	34	6.53	1.03	3−20−15−2	32	3.89	0.21
10−30−2	7	4.32	1.08	3−20−20−2	27	3.58	0.25
15−3−2	45	4.38	0.89	3−20−25−2	6	3.60	0.28
15−5−2	2	4.39	0.95	3−20−30−2	47	3.50	0.30
15−10−2	31	4.56	0.92	3−25−5−2	4	3.60	0.22
15−15−2	18	4.51	0.89	3−25−10−2	50	3.68	0.24
15−20−2	24	4.23	1.03	3−25−15−2	23	3.59	0.28
15−25−2	36	4.51	1.08	3−25−20−2	7	3.39	0.20
15−30−2	36	4.33	1.02	3−25−25−2	34	3.57	0.24
20−3−2	10	4.87	0.85	3−25−30−2	42	3.60	0.22
20−5−2	42	4.23	0.89	3−30−5−2	12	3.68	0.26
20−10−2	42	4.03	0.92	3−30−10−2	50	3.79	0.21
20−15−2	8	4.44	0.95	3−30−15−2	48	3.75	0.29
20−20−2	43	4.16	0.87	3−30−20−2	21	3.84	0.24
20−25−2	25	4.27	1.03	3−30−25−2	6	4.02	0.22
20−30−2	26	4.87	1.02	3−30−30−2	25	4.05	0.24
25−3−2	13	4.19	0.97				
25−5−2	26	4.55	0.92				
25−10−2	39	4.02	0.87				
25−15−2	11	3.89	0.96				
25−20−2	49	3.87	0.93				
25−25−2	27	4.02	1.05				
25−30−2	5	3.82	0.78				

the PR EoS generates better results (more accurate) with a smaller error in the vapor phase composition and the system pressure. In fact, some systems only can be modeled with the implementation of the VT-PR EoS. The same improvement can be observed in some systems with fatty acids and esters and in the system constituted by an alcohol solvent and glycerol. However, certain systems, as CO_2 + ethyl linoleate, CO_2 + DHA ethyl ester, and CO_2 + EPA ethyl ester, the PR EoS provides better results (more accurate when compared with experimental data) than the VT-PR EoS. These results may mean that the parameters N and k_3 of the VT-PR EoS were obtained with values of vapor pressure and specific volume of saturated liquid with a small accuracy or the critical properties of the components of the systems used in the thermodynamic modeling are not appropriate.

Nevertheless, the results provided by the VT-PR EoS, in most cases, are more accurate than the ones provided by the PR EoS, generating a better adjustment of the experimental data with optimum values of k_{ij} and l_{ij}.

DOI: 10.1021/acs.iecr.7b04195
Ind. Eng. Chem. Res. 2018, 57, 751−767

Table 13. Results for 5−*X*−*X*−2 and 10−*X*−*X*−2 Architectures

architecture	iteration	ΔP	Δy_1	architecture	iteration	ΔP	Δy_1
5−3−5−2	41	4.53	0.31	10−3−5−2	32	2.89	0.13
5−3−10−2	24	4.23	0.28	10−3−10−2	40	2.58	0.09
5−3−15−2	5	4.20	0.21	10−3−15−2	16	2.23	0.10
5−3−20−2	22	4.28	0.23	10−3−20−2	50	2.07	0.06
5−3−25−2	42	4.23	0.24	10−3−25−2	8	1.89	0.05
5−3−30−2	11	4.14	0.19	10−3−30−2	20	1.80	0.04
5−5−5−2	26	4.19	0.14	10−5−5−2	15	1.57	0.05
5−5−10−2	27	4.03	0.16	10−5−10−2	38	1.35	0.12
5−5−15−2	16	4.15	0.18	10−5−15−2	22	1.48	0.03
5−5−20−2	12	3.89	0.13	10−5−20−2	48	1.30	0.02
5−5−25−2	34	3.76	0.12	10−5−25−2	12	1.26	0.04
5−5−30−2	41	3.81	0.10	10−5−30−2	35	1.20	0.02
5−10−5−2	4	3.52	0.09	10−10−5−2	38	1.07	0.05
5−10−10−2	12	3.62	0.07	10−10−10−2	22	1.03	0.08
5−10−15−2	48	3.48	0.11	10−10−15−2	43	0.89	0.07
5−10−20−2	26	3.52	0.09	10−10−20−2	23	0.98	0.06
5−10−25−2	39	3.45	0.06	10−10−25−2	7	0.86	0.07
5−10−30−2	31	3.42	0.08	10−10−30−2	26	0.95	0.05
5−15−5−2	41	3.33	0.07	10−15−5−2	28	1.01	0.04
5−15−10−2	50	3.21	0.07	10−15−10−2	47	0.88	0.06
5−15−15−2	8	3.12	0.10	10−15−15−2	27	0.83	0.10
5−15−20−2	36	3.05	0.08	10−15−20−2	44	1.02	0.12
5−15−25−2	6	3.15	0.12	10−15−25−2	45	0.98	0.05
5−15−30−2	39	2.89	0.14	10−15−30−2	49	1.14	0.07
5−20−5−2	40	2.81	0.09	10−20−5−2	4	1.28	0.07
5−20−10−2	26	2.57	0.09	10−20−10−2	48	1.25	0.04
5−20−15−2	38	2.69	0.07	10−20−15−2	24	1.33	0.03
5−20−20−2	24	2.61	0.12	10−20−20−2	38	1.43	0.03
5−20−25−2	35	2.83	0.08	10−20−25−2	38	1.50	0.05
5−20−30−2	25	2.98	0.11	10−20−30−2	48	1.68	0.04
5−25−5−2	18	3.03	0.13	10−25−5−2	48	1.60	0.12
5−25−10−2	14	3.15	0.10	10−25−10−2	11	1.66	0.07
5−25−15−2	1	3.01	0.12	10−25−15−2	30	1.63	0.05
5−25−20−2	48	3.21	0.10	10−25−20−2	40	1.75	0.09
5−25−25−2	19	3.04	0.10	10−25−25−2	10	1.72	0.06
5−25−30−2	1	3.27	0.09	10−25−30−2	2	1.82	0.08
5−30−5−2	15	3.31	0.13	10−30−5−2	20	1.80	0.06
5−30−10−2	29	3.24	0.11	10−30−10−2	44	1.78	0.06
5−30−15−2	41	3.45	0.08	10−30−15−2	3	1.89	0.07
5−30−20−2	41	3.48	0.13	10−30−20−2	49	2.01	0.10
5−30−25−2	26	3.52	0.14	10−30−25−2	34	2.04	0.06
5−30−30−2	45	3.50	0.09	10−30−30−2	45	2.11	0.04

3.5. Thermodynamic Simulation. *3.5.1. SMILES code.* The SMILES codes obtained are shown in Table 10.

3.5.2. Molecular Descriptor. Numeric values of the molecular descriptors, obtained by using the SMILES codes (Table 10) in Dragon 7.0, are shown in Table 11.

3.5.3. Artificial Neural Networks. The shortage of data about the vapor−liquid equilibrium of biodiesel systems using ANN was the reason to investigate an optimum architecture through trial and error. Different architectures were obtained combining different numbers of nodes among the layers. At first, configurations with three layers (*X*−*X*−2) and then configurations with four layers (X−*X*−*X*−2) were analyzed, to find the most accurate one for this study.

All data are used independently of the compounds present in the binary systems. These data (367) are arranged randomly for a better prediction capability and divided into three groups according to the three steps that constitute the thermodynamic simulation, shown in Figure 2: learning (300), testing (40), and predicting (27). The type of ANN employed was the feed-forward back-propagation; the error between one iteration and the next one was set to 0.0001, the maximum of iterations was set to 500, and the program ran 50 times using the Levenberg−Marquardt algorithm.

The results of the thermodynamic simulation are presented in Tables 12 (configurations *X*−*X*−2 and 3−*X*−*X*−2) and 13 (configurations 5−*X*−*X*−2 and 10−*X*−*X*−2), respectively. The average absolute deviations, $|\Delta P|$ and $|\Delta y_1|$, for a set of N data were defined as

$$|\Delta \mathrm{DV}| = \frac{100}{N}\sum_{1}^{N}\frac{|(\mathrm{DV})^{\mathrm{pred}} - (\mathrm{DV})^{\mathrm{exp}}|_i}{(\mathrm{DV})_i^{\mathrm{pred}}} \quad (32)$$

where DV represents each dependent variable: system pressure, P (bar), and vapor phase composition, y_1.

DOI: 10.1021/acs.iecr.7b04195
Ind. Eng. Chem. Res. 2018, 57, 751−767

Table 14. Some Average Individual Deviations for the System Pressure (MPa) and Vapor Phase Composition in the Testing Step for the Architecture 10−10−25−2

binary system		experimental			experimental		testing step		% deviation	
biodiesel component (T_c, P_c, w)	supercritical solvent (1) (T_c, P_c, w)	T (K)	x_1	MD	P (MPa)	y_1	P (MPa)	y_1	ΔP	Δy_1
EPA ethyl ester	CO_2	323.2	0.6437	–	0.513	0.9999	0.520	0.9982	0.77	0.17
tripalmitin	CO_2	353.2	0.8324	–	0.562	0.9984	0.551	0.9952	1.09	0.32
caproic acid	CO_2	313.2	0.9110	–	0.853	0.9989	0.862	0.9953	1.40	0.36
methyl myristate	methanol	543.0	0.8290	–	0.527	0.9993	0.524	0.9971	0.77	0.22
palmitic acid	CO_2	373.2	0.7063	–	2.496	0.9999	2.470	0.9973	0.85	0.26
C18 methyl esters	methanol	573.0	0.8600	–	1.155	0.9860	1.143	0.9831	0.79	0.29
triolein	methanol	493.0	0.9755	–	0.494	0.9997	0.470	0.9970	2.97	0.27
ethyl oleate	CO_2	333.2	0.8180	–	1.215	0.9990	1.202	0.9965	0.83	0.25
tristearin	CO_2	333.0	0.8770	–	3.304	0.9997	3.251	0.9958	1.51	0.39
ethyl laurate	ethanol	523.0	0.8340	–	0.480	0.9983	0.482	0.9968	1.04	0.15
methyl laurate	methanol	523.0	0.5870	–	0.434	0.9991	0.443	0.9973	1.38	0.18
glycerol	methanol	543.0	0.5920	–	0.703	0.9999	0.711	0.9966	1.27	0.33
ethyl linoleate	CO_2	313.2	0.5820	–	0.430	1.0000	0.440	0.9978	1.15	0.22
DHA ethyl ester	CO_2	323.2	0.8664	–	1.441	0.9964	1.462	0.9940	1.23	0.24
glycerol	ethanol	523.0	0.4550	–	0.332	0.9999	0.323	0.9956	2.19	0.43
									1.28	0.27

Table 15. Some Average Individual Deviations for the System Pressure (MPa) and the Vapor Phase Composition in the Prediction Step for the Architecture 10−10−25−2

binary system		experimental			experimental		prediction step		% deviation	
biodiesel component (T_c, P_c, w)	supercritical solvent (1) (T_c, P_c, w)	T (K)	x_1	MD	P (MPa)	y_1	P (MPa)	y_1	ΔP	Δy_1
methyl laurate	methanol	493.2	0.4139	–	0.201	0.9997	0.193	0.9988	1.46	0.09
triolein	CO_2	353.0	0.8360	–	2.282	1.0000	2.264	0.9990	1.23	0.10
EPA ethyl ester	CO_2	333.2	0.7777	–	1.040	1.0000	1.031	0.9988	1.18	0.12
ethyl stearate	CO_2	313.2	0.8460	–	0.962	0.9988	0.952	0.9968	1.12	0.20
DHA ethyl ester	CO_2	313.2	0.8717	–	1.140	0.9940	1.140	0.9929	0.56	0.11
tristearin	CO_2	353.0	0.8830	–	0.713	1.0000	0.711	0.9989	0.73	0.11
ethyl oleate	CO_2	333.2	0.6860	–	2.082	0.9698	2.062	0.9673	0.99	0.25
lauric acid	CO_2	333.2	0.8529	–	0.401	0.9997	0.392	0.9979	1.23	0.18
ethyl myristate	ethanol	543.0	0.5520	–	0.370	0.9998	0.361	0.9981	1.58	0.17
glycerol	ethanol	493.0	0.8330	–	1.514	0.9864	1.500	0.9840	0.72	0.24
ethyl linoleate	CO_2	333.2	0.9090	–	0.712	0.9999	0.703	0.9971	1.21	0.28
C18 methyl esters	methanol	573.0	0.6070	–	2.002	0.9673	1.982	0.9650	0.36	0.24
methyl myristate	methanol	523.0	0.3900	–	4.071	0.9991	4.094	0.9973	0.50	0.18
tripalmitin	CO_2	333.0	0.9120	–	0.810	0.9924	0.811	0.9911	0.90	0.13
triolein	methanol	433.2	0.7300	–	0.812	0.9994	0.800	0.9969	1.12	0.25
									0.99	0.18

The best result depends on the selection of appropriate data, the choice of a good architecture, and variables capable of generating adequate correlation and prediction of thermodynamic properties. The interpretation of the average absolute deviation and the lowest maximum absolute deviation led to the architecture 10−10−25−2 found at the seventh run, as shown in Table 13.

In the learning step, individual absolute deviations between correlated and experimental values were below 1.5% for the most of the data. For the system pressure, 15 points showed absolute deviations greater than 3.0%, with 4.5% the highest value. For the vapor phase composition, 10 points showed absolute deviations greater than 0.8% (1.0% for the highest value), while all of the other 290 points gave absolute deviations below than 0.7%. Average absolute deviations for the system pressure and the vapor phase composition were 1.35 and 0.38%, respectively. These values were considered accurate enough to say that the ANN learned successfully.

Once the optimum network architecture was determined in the learning step, 40 and 27 input data (independent variables) of the biodiesel systems, not used in the previous process, were included in the third and fifth worksheets of the Excel file, respectively, and were read by the computer program. Some of the tested (15 points) and predicted (15) values of the system pressure and the vapor phase composition are shown in Tables 14 and 15.

Table 14 shows the average individual absolute deviations for the system pressure and the vapor phase composition tested by the proposed ANN architecture for points (40) not used during the learning step. Testing results were done at conditions used during the learning process. The optimum configuration reproduced the system pressure with absolute deviations below 1.51%, except in two cases, in which absolute deviations were below 3.00%. For the vapor phase composition, the absolute deviations were below 0.40% and, in only one case, the absolute deviation was below 0.43%. In testing step, the average total

DOI: 10.1021/acs.iecr.7b04195
Ind. Eng. Chem. Res. 2018, 57, 751−767

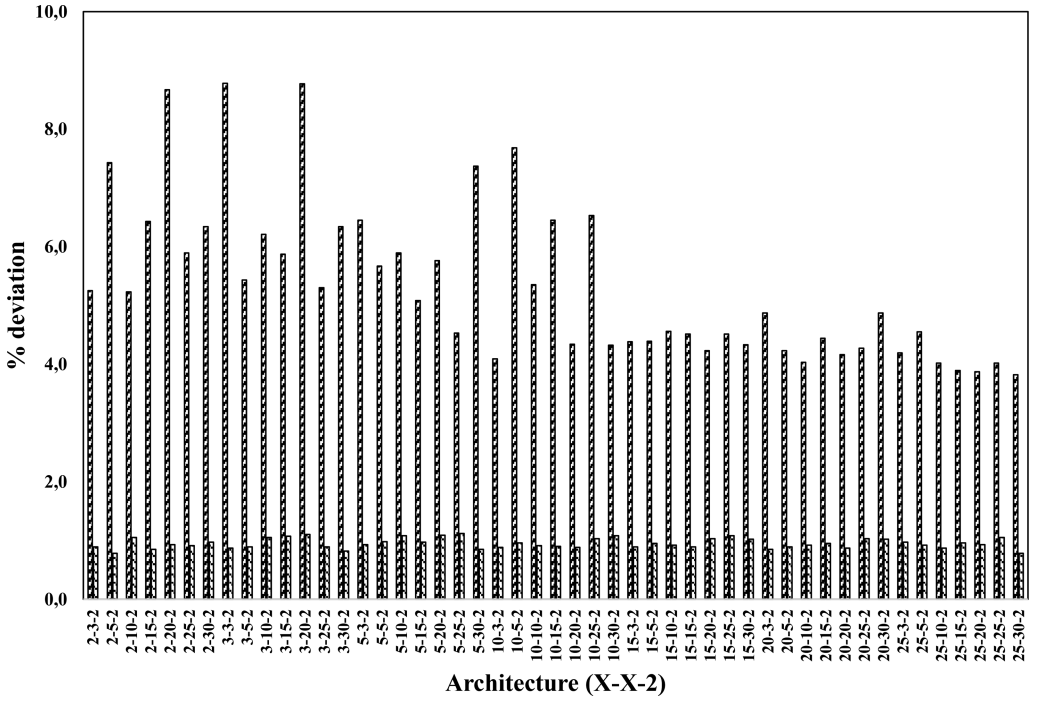

Figure 3. Deviations for the pressure (▨) and vapor phase composition (▧) for architectures of type *X*−*X*−2.

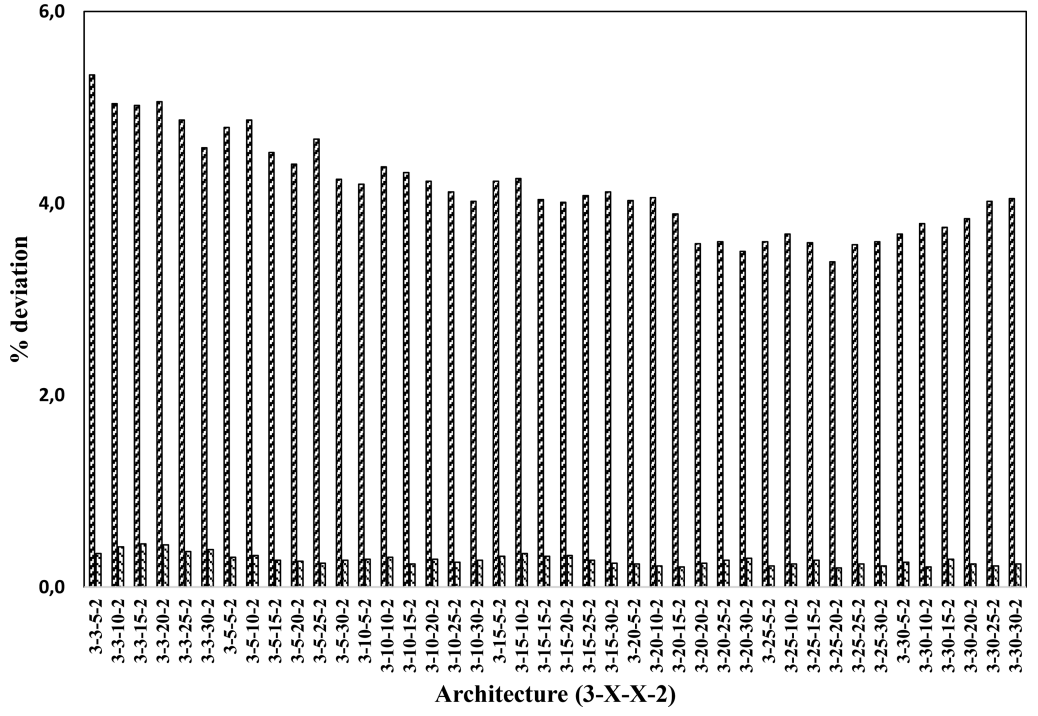

Figure 4. Deviations for the pressure (▨) and vapor phase composition (▧) for architectures of type 3−*X*−*X*−2.

absolute deviations for the system pressure and the vapor phase composition were 1.28 and 0.27%, respectively.

Table 15 shows the average absolute deviations for the system pressure and the vapor phase composition predicted for data not used in the two previous steps by the best-selected model. The optimum ANN model reproduced the system pressure and the vapor phase composition of the fluid phase behavior of the vapor−liquid equilibrium of biodiesel systems at supercritical conditions with average absolute deviations of 0.99 and 0.18%, respectively. The maximum individual absolute deviation in predicting the system pressure was 1.58%. With respect to the vapor phase composition, this property was predicted with average absolute deviations from 0.09 to 0.28%.

In Figures 3−6 were plotted the results obtained for the predicting step of system pressure and the vapor phase composition for all configurations studied in this work. As mentioned, the optimum architecture found was the four-layer configuration 10−10−25−2 (Figure 6).

DOI: 10.1021/acs.iecr.7b04195
Ind. Eng. Chem. Res. 2018, 57, 751−767

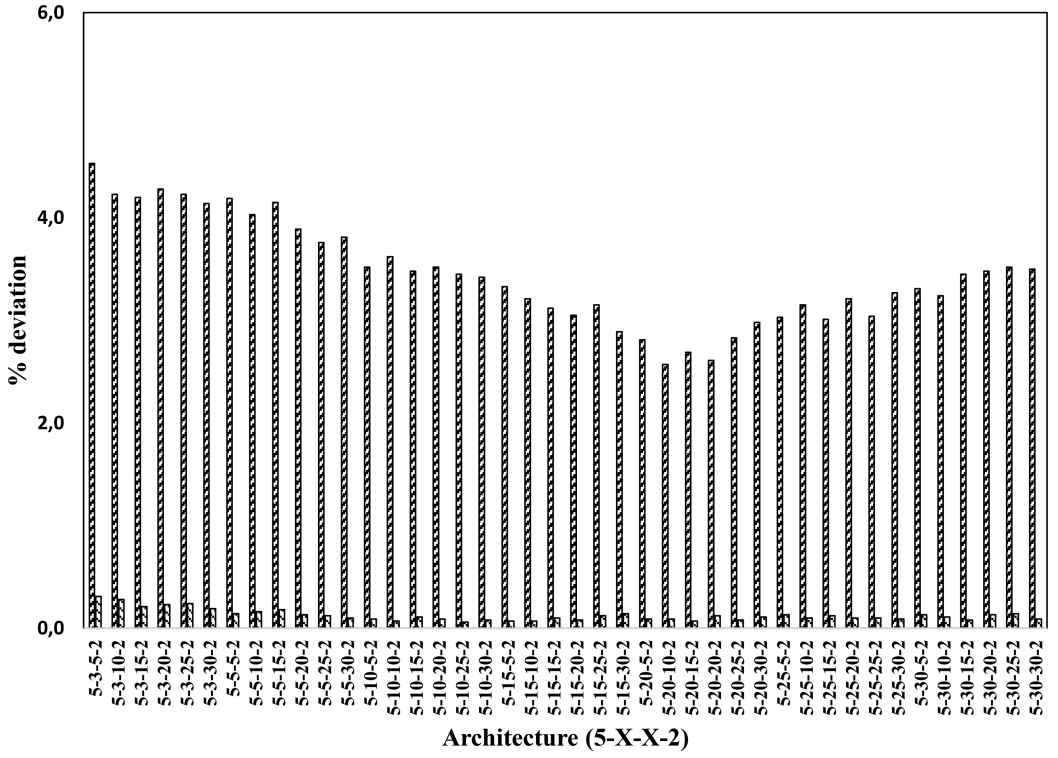

Figure 5. Deviations for the pressure (▨) and vapor phase composition (▧) for architectures of type 5−*X*−*X*−2.

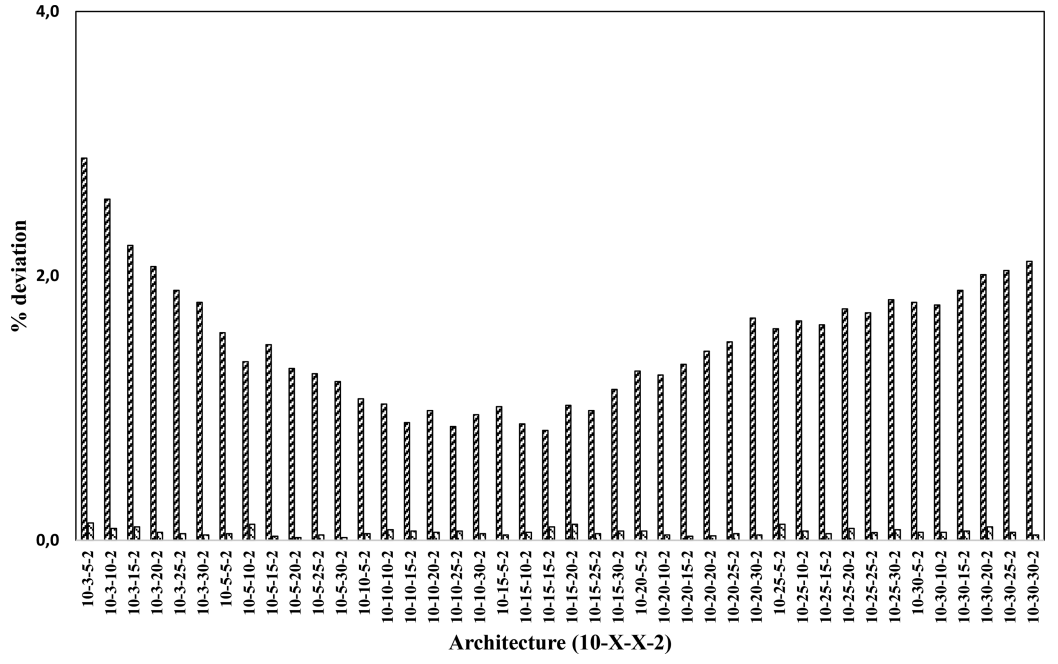

Figure 6. Deviations for the pressure (▨) and vapor phase composition (▧) for architectures of type 10−*X*−*X*−2.

In Figures 7−10 are shown the predicted results of the fluid phase behavior of the vapor−liquid equilibrium of binary systems at supercritical conditions involving solvents and biodiesel components. These results were obtained by using the cubic equations of state, PR and VT-PR, and the noncubic equation of state, PC-SAFT, all of them with adjustable parameters determined previously and the ones obtained with ANN with the 10−10−25−2 architecture. Figures 7−10 show the excellent agreement between the experimental data and the PC-SAFT EoS and the ANN predicted data. The great difference between the thermodynamic modeling and thermodynamic simulation is the processing time. As for thermodynamic modeling, it is necessary to adjust binary interaction parameters for each system at several temperatures; the thermodynamic simulation performed with artificial neural networks and molecular descriptors involves the data of all binary systems at once.

4. CONCLUSIONS

In this work, the fluid phase behavior of binary systems involving solvents and biodiesel components at supercritical conditions

DOI: 10.1021/acs.iecr.7b04195
Ind. Eng. Chem. Res. 2018, 57, 751−767

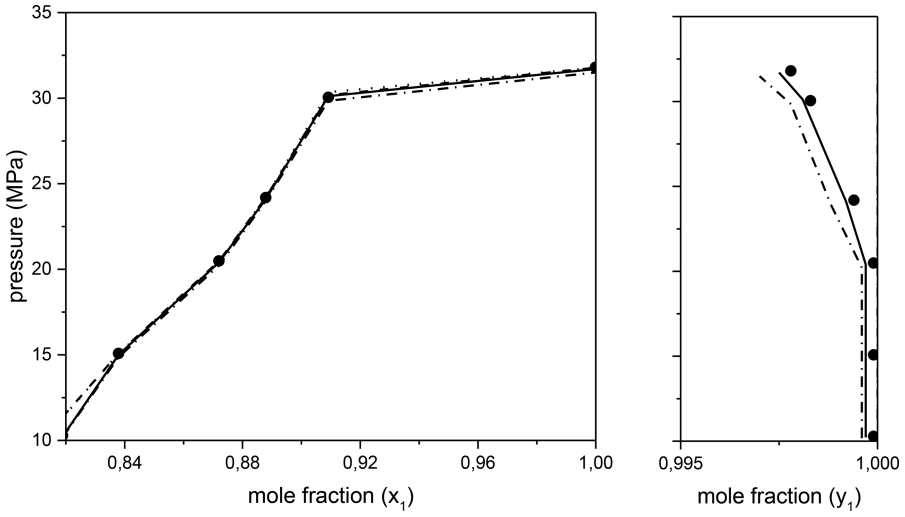

Figure 7. Comparison between experimental data (●) and the predicted phase equilibrium diagram using PR (···), VT-PR (---), and PC-SAFT (– · –) equations of state and ANN model (—) for CO_2 (1) + trilaurin (2) (T = 353.15 K).

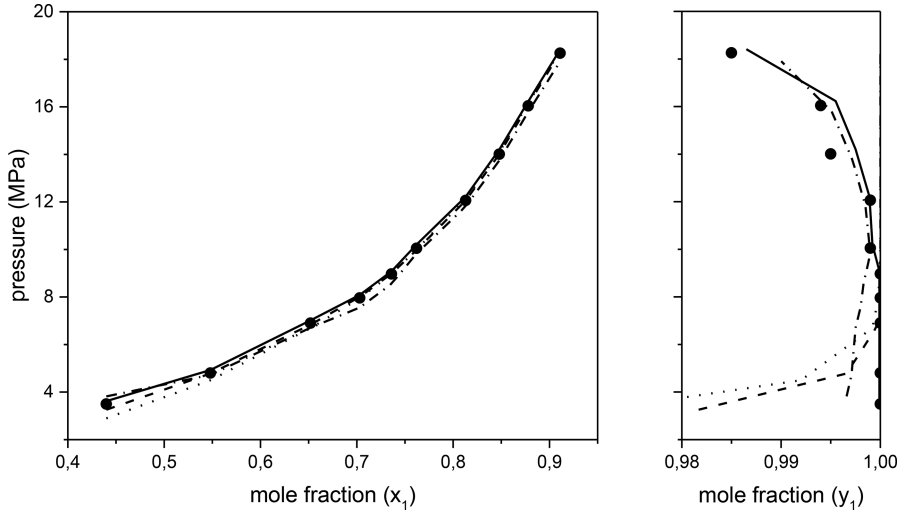

Figure 8. Comparison between experimental data (●) and the predicted phase equilibrium diagram using PR (···), VT-PR (---), and PC-SAFT (– · –) equations of state and ANN model (—) for CO_2 (1) + ethyl stearate (2) (T = 333.15 K).

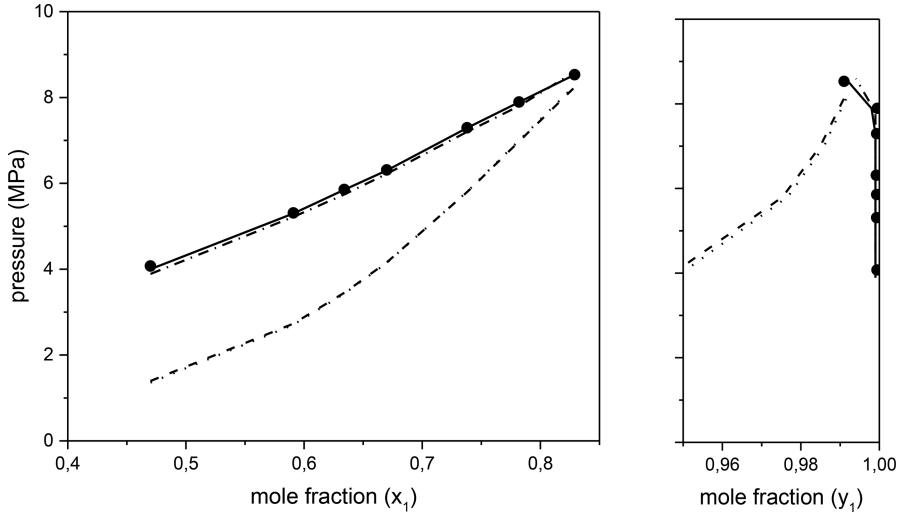

Figure 9. Comparison between experimental data (●) and the predicted phase equilibrium diagram using PR (···), VT-PR (---), and PC-SAFT (– · –) equations of state and ANN model (—) for methanol (1) + methyl myristate (2) (T = 543.15 K).

DOI: 10.1021/acs.iecr.7b04195
Ind. Eng. Chem. Res. 2018, 57, 751–767

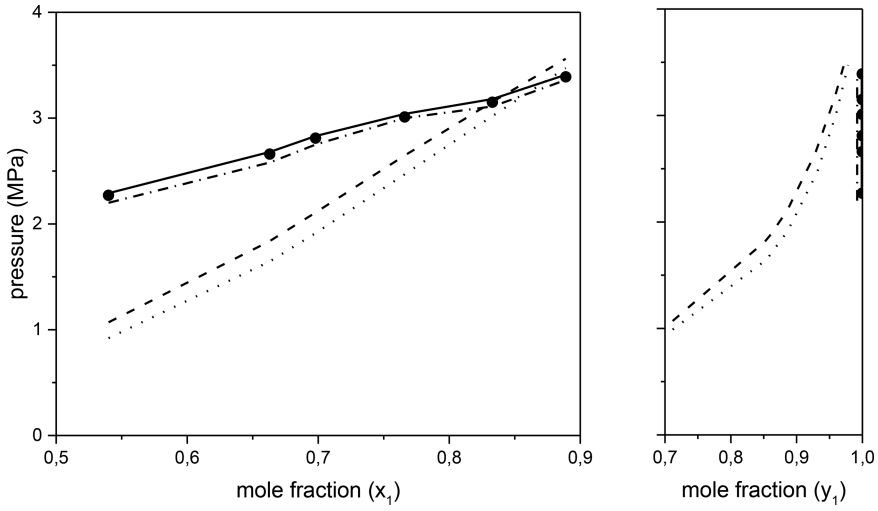

Figure 10. Comparison between experimental data (●) and the predicted phase equilibrium diagram using PR (···), VT-PR (---), and PC-SAFT (— · —) equations of state and ANN model (—) for ethanol (1) + glycerol (2) (T = 493.15 K).

was studied by comparing the performance between the thermodynamic modeling (cubic and noncubic equations of state) and simulation (ANN + molecular descriptors). Pure component parameters for the VT-PR EoS, N and k_3, were obtained using the vapor pressure and the specific volume of the saturated liquid of each component. For the PR and VT-PR models, the vdW2 mixing rule was used and the binary interaction parameters were obtained as a function of temperature. Experimental data points of all binary systems considered thermodynamically inconsistent were very few.

Thermodynamic models, used in this work, adjusted appropriately the experimental data studied for the most cases by using the bubble pressure method and the ϕ–ϕ approach. However, the PR and VT-PR equations of state, at some conditions, were not able to predict the vapor phase. The PC-SAFT correlation fitted the all vapor–liquid equilibrium data with a good accuracy. In this work an artificial neural network model has been used to predict the bubble point (BUBL P) by using molecular descriptors. Results obtained by the ANN with molecular descriptors, for the best architecture (10–10–25–2), have given an overall agreement between experimental and prediction values for the thermodynamic consistency data. With this configuration, the training and prediction results are very close to the experimental data, being that the absolute average deviations for the bubble pressure and the vapor phase compositions are 1.28 and 0.27% for the training step and 0.99 and 0.18% for the prediction step.

AUTHOR INFORMATION

Corresponding Author

*Tel.: +55-12-31595326. Fax: +55-12-31595017. E-mail: parce@usp.br (P.F. Arce).

ORCID

Pedro F. Arce: 0000-0002-4687-5297

Notes

The authors declare no competing financial interest.

ACKNOWLEDGMENTS

The financial support of the Fundação de Amparo à Pesquisa do Estado de São Paulo, FAPESP (Brazil), and the Conselho Nacional de Desenvolvimento Cientifico e Tecnológico, CNPq (Brazil), through Grants 2015/05155-8 and 158824/2015-6, respectively, are gratefully acknowledged.

ABBREVIATIONS

ANN = artificial neural networks
EoS = equation of state
MD = molecular descriptors
PC-SAFT = perturbed chain statistical associating fluid theory
PR = Peng–Robinson
SMILES = Simplified Molecular Input Line Entry System
vdW2 = van der Waals 2
VT-PR = volume-translated Peng–Robinson

REFERENCES

(1) Madras, G.; Kolluru, C.; Kumar, R. Synthesis of biodiesel in supercritical fluids. *Fuel* **2004**, *83*, 2029.

(2) Kusdiana, D.; Saka, S. Effects of water on biodiesel fuel production by supercritical methanol treatment. *Bioresour. Technol.* **2004**, *91*, 289.

(3) Tan, K. T.; Lee, K. T. A review on supercritical fluids (SCF) technology in sustainable biodiesel production: potential and challenges. *Renewable Sustainable Energy Rev.* **2011**, *15*, 2452.

(4) Pinnarat, T.; Savage, P. E. Assessment of noncatalytic biodiesel synthesis using supercritical reaction conditions. *Ind. Eng. Chem. Res.* **2008**, *47*, 6801.

(5) Kalra, H.; Krishnana, T. R.; Robinson, D. B. Equilibrium-phase properties of carbon dioxide–n-butane and nitrogen–hydrogen sulfide systems at subambient temperatures. *J. Chem. Eng. Data* **1976**, *21*, 222.

(6) da Silva, I. N.; Spatti, D. N.; Flauzino, R. A.; Liboni, L. H.; Alves, S. F. *Artificial Neural Networks – A Practical Course*; Springer International Publishing Switzerland: 2017.

(7) Kim, P. *MATLAB Deep Learning: With Machine Learning, Neural Networks and Artificial Intelligence*; Apress: Seoul, Korea, 2017.

(8) *MatLab*, version R2016b; MathWorks: Natick, MA, USA, 2016.

(9) Todeschini, R.; Consonni, V. *Handbook of Molecular Descriptors*; Wiley-VCH: Weinheim, Germany, 2000.

(10) Danishuddin, A.; Khan, A. U. Descriptors and their selection methods in QSAR analysis: paradigm for drug design. *Drug Discovery Today* **2016**, *21*, 1291.

(11) Kode SRL. *Dragon (Software for Molecular Descriptor Calculation)*, version 7.0; 2016. http://chm.kode-solutions.net.

(12) Weininger, D. SMILES, a chemical language and information system. 1. Introduction to methodology and encoding rules. *J. Chem. Inf. Model.* **1988**, *28*, 31.

(13) Weininger, D.; Weininger, A.; Weininger, J. L. SMILES. 2. Algorithm for generation of unique SMILES notation. *J. Chem. Inf. Model.* **1989**, *29*, 97.

(14) Peng, D. Y.; Robinson, D. B. A new two-constant equation of state. *Ind. Eng. Chem. Fundam.* **1976**, *15*, 59.

DOI: 10.1021/acs.iecr.7b04195
Ind. Eng. Chem. Res. 2018, 57, 751–767

(15) Tsai, J. C.; Chen, Y. P. Application of a volume-translated Peng-Robinson equation of state on vapor-liquid equilibrium calculations. *Fluid Phase Equilib.* **1998**, *145*, 193.
(16) Gross, J.; Sadowski, G. Application of perturbation theory to a hard-chain reference fluid: an equation of state for square-well chains. *Fluid Phase Equilib.* **2000**, *168*, 183.
(17) Gross, J.; Sadowski, G. Perturbed-chain SAFT: an equation of state based on a perturbation theory for chain molecules. *Ind. Eng. Chem. Res.* **2001**, *40*, 1244.
(18) Chapman, W. G.; Jackson, G.; Gubbins, K. E. Phase equilibria of associating fluids: chain molecules with multiple bonding sites. *Mol. Phys.* **1988**, *65*, 1057.
(19) Chapman, W. G.; Gubbins, K. E.; Jackson, G.; Radosz, M. New reference equation of state for associating liquids. *Ind. Eng. Chem. Res.* **1990**, *29*, 1709.
(20) Barker, J. A.; Henderson, D. Perturbation theory and equation of state for pure fluids: the square-well potential. *J. Chem. Phys.* **1967**, *47*, 2856.
(21) Arce, P.; Aznar, M. Modeling of binary and ternary mixture critical lines using non-cubic and cubic equations of state. *J. Supercrit. Fluids* **2007**, *42*, 1.
(22) Gross, J.; Sadowski, G. Application of the Perturbed-Chain SAFT equation of state to associating systems. *Ind. Eng. Chem. Res.* **2002**, *41*, 5510.
(23) Michelsen, M. L.; Mollerup, J. M. *Thermodynamic Models: Fundamentals & Computational Aspects*, 2nd ed.; Tie-Line Publications: Holte, Denmark, 2007.
(24) Prausnitz, J. M.; Lichtenthaler, R. N.; de Azevedo, E. C. *Molecular Thermodynamics of Fluid-Phase Equilibria*, 3rd ed.; Prentice Hall PTR: Upper Saddle River, NJ, USA, 1999.
(25) Arce, P.; Aznar, M. Computation and modeling of tricritical phenomena in ternary and quaternary mixtures using the Perturbed Chain—Statistical Associating Fluid Theory equation of state. *J. Supercrit. Fluids* **2009**, *49*, 135.
(26) Álvarez, V. H.; Aznar, M. Application of a thermodynamic consistency test to binary mixtures containing an ionic liquid. *Open Thermodyn. J.* **2008**, *2*, 25.
(27) Valderrama, J. O.; Forero, L. A.; Rojas, R. E. Critical properties and normal boiling temperature of ionic liquids. Update and a new consistency test. *Ind. Eng. Chem. Res.* **2012**, *51*, 7838.
(28) Jackson, P. L.; Wilsak, R. A. Thermodynamic consistency tests based on the Gibbs-Duhem equation applied to isothermal, binary vapor-liquid equilibrium data: data evaluation and model testing. *Fluid Phase Equilib.* **1995**, *103*, 155.
(29) Mohammadi, A. H.; Eslamimanesh, A.; Richon, D. Wax solubility in gaseous system: thermodynamic consistency test of experimental data. *Ind. Eng. Chem. Res.* **2011**, *50*, 4731.
(30) Wisniak, J.; Ortega, J.; Fernández, L. A fresh look at the thermodynamic consistency of vapour-liquid equilibria data. *J. Chem. Thermodyn.* **2017**, *105*, 385.
(31) Arce, P. F.; Vilella, G. A.; Valderrama, J. O. Prediction of critical pressure of ionic liquids (Imidazolium) utilizing artificial neural networks. Presented at the 5th Iberoamerican Meeting on Ionic Liquids, Santos, Brazil, 2017.
(32) Bharath, R.; Yamane, S.; Inomata, H.; Adschiri, T.; Arai, K. Phase equilibria of supercritical CO2 − fatty oil component binary systems. *Fluid Phase Equilib.* **1993**, *83*, 183.
(33) Weber, W.; Petkov, S.; Brunner, G. Vapour-liquid equilibria and calculations using the Redlich-Kwong-Aspen-equation of state for tristearin, tripalmitin, and triolein in CO_2 and propane. *Fluid Phase Equilib.* **1999**, *158−160*, 695.
(34) Glisic, S.; Montoya, O.; Orlovic, A.; Skala, D. Vapor-liquid equilibria of triglycerides-methanol mixtures and their influence on the biodiesel synthesis under supercritical conditions of methanol. *J. Serb. Chem. Soc.* **2007**, *72*, 13.
(35) Bharath, R.; Inomata, H.; Arai, K.; Shoji, K.; Noguchi, Y. Vapor-liquid equilibria for binary mixtures of carbon dioxide and fatty acid ethyl esters. *Fluid Phase Equilib.* **1989**, *50*, 315.
(36) Shimoyama, Y.; Iwai, Y.; Abeta, T.; Arai, Y. Measurement and correlation of vapor-liquid equilibria for ethanol + ethyl laurate and ethanol + ethyl myristate systems near critical temperature of ethanol. *Fluid Phase Equilib.* **2008**, *264*, 228.
(37) Shimoyama, Y.; Iwai, Y.; Jin, B. S.; Hirayama, T.; Arai, Y. Measurement and correlation of vapor-liquid equilibria for methanol + methyl laurate and methanol + methyl myristate systems near critical temperature of methanol. *Fluid Phase Equilib.* **2007**, *257*, 217.
(38) Fang, T.; Shimoyama, Y.; Abeta, T.; Iwai, Y.; Sasaki, M.; Goto, M. Phase equilibria for the mixtures of supercritical methanol + C18 methyl esters and supercritical methanol + α-tocopherol. *J. Supercrit. Fluids* **2008**, *47*, 140.
(39) Shimoyama, Y.; Abeta, T.; Zhao, L.; Iwai, Y. Measurement and calculation of vapor-liquid equilibria for methanol + glycerol and ethanol + glycerol systems at 493−573 K. *Fluid Phase Equilib.* **2009**, *284*, 64.
(40) Cruz, M. S.; Aca, G. A.; Daza, O. S.; Arenas, T. L. Predicting critical properties, density and viscosity of fatty acids, triacylglycerides and methyl esters by group contribution methods. Presented at the 20th European Symposium on Computer Aided Process Engineering, 2010.
(41) *DIPPR Information and Data Evaluation Manager*, version 1.2.0; 2000.
(42) Costa, M. C.; Boros, L. A. D.; Batista, M. L. S.; Coutinho, J. A. P.; Krähenbühl, M. A.; Meirelles, A. J. A. Phase diagrams of mixtures of ethyl palmitate with fatty acid ethyl esters. *Fuel* **2012**, *91*, 177.
(43) Karim, A. M. A.; Mutlag, A. K.; Hameed, M. S. Vapor-liquid equilibrium prediction by PE and ANN for extraction of unsaturated fatty acid esters by supercritical CO_2. *ARPN J. Eng. Appl. Sci.* **2011**, *6* (9), 122.
(44) Wallek, T.; Rarey, J.; Metzger, J. O.; Gmehling, J. Estimation of pure-component properties of biodiesel-related components: fatty acid methyl esters, fatty acids and triglycerides. *Ind. Eng. Chem. Res.* **2013**, *52*, 16966.
(45) *Ullman's Food and Feed*; Wiley-VCH: Weinheim, Germany, 2017; Vol. *1*.
(46) Goodrum, J. W.; Geller, D. P. Rapid thermogravimetric measurements of boiling points and vapor pressure of saturated medium- and long-chain triglycerides. *Bioresour. Technol.* **2002**, *84*, 75.
(47) Silva, L. Y. A.; Falleiro, R. M. M.; Meirelles, A. J. A.; Krähenbühl, M. A. Determination of the vapor pressure of ethyl esters by differential scanning calorimetry. *J. Chem. Thermodyn.* **2011**, *43*, 943.
(48) Pratas, M. J.; Freitas, S.; Oliveira, M. B.; Monteiro, S. C.; Lima, A. S.; Coutinho, J. A. P. Densities and viscosities of fatty acid methyl and ethyl esters. *J. Chem. Eng. Data* **2010**, *55*, 3983.
(49) Pratas, M. J.; Freitas, S.; Oliveira, M. B.; Monteiro, S. C.; Lima, A. S.; Coutinho, J. A. P. Densities and viscosities of minority fatty acid methyl and ethyl esters present in biodiesel. *J. Chem. Eng. Data* **2011**, *56*, 2175.
(50) Mishra, V. K.; Temelli, F.; Ooraikul, B. Vapor pressure of fatty acid esters: correlation and estimation. *J. Food Eng.* **1994**, *23*, 467.
(51) *NIST Chemistry WebBook, NIST Standard Reference Database 69*; Linstrom, P. J., Mallard, W. G., Eds.; National Institute of Standards and Technology: Gaithersburg, MD, 2017.
(52) Stragevitch, L.; d'Avila, S. G. Application of a generalized maximum likelihood method in the reduction of multicomponent liquid-liquid equilibrium data. *Braz. J. Chem. Eng.* **1997**, *14*, 41.
(53) Igarashi, E. M. S. Thermodynamic modeling, consistency and simulation of the vapor-liquid phase behavior of binary systems containing components present in the biodiesel production (in Portuguese). M.S. Dissertation, Engineering School of Lorena, University of São Paulo, 2017.

DOI: 10.1021/acs.iecr.7b04195
Ind. Eng. Chem. Res. 2018, 57, 751−767